Moroccan Journal of Chemistry
ISSN: 2351-812X
http://revues.imist.ma/?journal=morjchem&page=login
El Bindary & al. / Mor. J. Chem. 8 N°3 (2020) 627-637

Equilibrium, Kinetic and Thermodynamic studies of adsorption of cationic dyes from aqueous solution using ZIF-8

N. Hassan[1], A. Shahat[2], A. El-Didamony[3], M.G. El-Desouky[1], A.A. El-Bindary[4*]

[1]*Chemistry Department, Faculty of Science, Port Said University, Port Said 42511, Egypt.*
[2]*Chemistry Department, Faculty of Science, Suez University, Suez 43518, Egypt.*
[3]*Chemistry Department, Faculty of Science, Zagazig University, Zagazig 44519, Egypt.*
[4]*Chemistry Department, Faculty of Science, Damietta University, Damietta 34517, Egypt.*

** Corresponding author:*
abindary@yahoo.com
Received 03 March 2020,
Revised 21 May 2020,
Accepted 23 June 2020

Abstract

Zeolitic imidazolate framework-8 (ZIF-8) is one type of (MOFs) that has been synthesized and characterized and detailed analysis of Crystal violet (CV) and Malachite Green (MG) adsorption behaviour. Impact of different variables on batch method as a function of solution pH, concentration of CV and MG, dose of ZIF-8, Contact time and temperature were analyzed and optimal test conditions were determined. Scanning electron microscopy (SEM) was used to measure surface alterations of the ZIF-8. The surface area and volume of the pores were found to be 495.199 m^2g^{-1} and 0.026 cm^3g^{-1}, respectively as determined by the Brunauer-Emmett-Teller (BET) test. ZIF-8 point of zero charging (pH_{PZC}) was calculated and was found 7.9. Adsorption data were modeled on isotherms for adsorption of Langmuir, Freundlich, Dubinin–Radushkevich and Temkin. Equilibrium data from the adsorption processes showed that the Langmuir is fitted with CV and MG adsorption. Pseudo-first order, pseudo-second order, kinetic models Weber and Morris and Elovich were used to analyze the kinetic data obtained at different initial dye concentrations. The kinetics of adsorption showed that the action in adsorption adopted the processes of pseudo-second - order kinetic model and chemisorption. The thermodynamic parameter such as ΔG, ΔS and ΔH has been determined. Study of thermodynamics for adsorption indicated the reaction was endothermal and spontaneous.

Keywords: *ZIF-8, Kinetic, Adsorption isotherm,* Thermodynamics, pH_{PZC} .

1. Introduction

Dyes were known to be the key component of sewage being one of the most chemical industries. More than 700,000 tons of dyes produced by textile factories are among the top three pollutants. Most of the reactive dyes are toxic and threaten teratogenic and carcinogenic mutations [1]. Compared to other water exchange methods, such as electrolysis, flocculation and photocatalysis [2]. The benefit of using porous adsorptive materials was high performance, low cost and easy recycling [3]. Nevertheless, it is theoretically important to track and adjust the sensitivity of the adsorbent surface to adsorb different types of dye molecules with a wide range of hydrophilicity or polarity. Hydroxyapatite, a typical adsorbent bio-composite [4]. Or the activated carbon adsorbent [5] has low potential for adsorption, and therefore hard to boost on the surface. While the emerging metal organic frameworks (MOFs) have superb functional versatility, which is useful for applications of separation and adsorption [6]. Tuning a MOF surface properties and controlling its development costs can contribute to new solutions to water pollution problems. The coloring is difficult to degrade and to extract from water. By extremely high porosity, structural flexibility, shape/size of the compositional and high tunable pores, and surface functionality. Adsorbent MOFs demonstrate good performance for extracting dye [7]. Metal–organic frameworks (MOFs) are crystalline porous materials well known for their different uses [8]. MOF materials are of particular interest because their surface area and pore size are simply tuned. Many MOFs, such as MIL-101, UiO-66 and MIL-53, have been tested as adsorbents to remove colors from water and have achieved modest adsorption capability [9]. Zeolitic imidazolate frameworks (ZIFs) form were considered one of the family of MOFs [10]. ZIF-8 is one of the most studied prototypical ZIF compounds, which are porous crystals constructed from imidazolate-bridged tetrahedral zinc ions, with extended three-dimensional structures. The aim of this study was to determine the effectiveness of ZIF-8 as an adsorbent to extract dangerous (MG) and (CV) dyes from aqueous solution. Experimental parameters influencing the adsorption process were evaluated, such as dosing adsorbents, pH, contact time, and temperature. Due to the well-scattered zinc ions within the pores and the wide surface area (495.199 m^2g^{-1}) ZIF-8 has highly efficient adsorbents for extracting water from MG and CV dyes. The experimental equilibrium adsorption effects were evaluated by kinetic and isotherm models.

2. Materials and Methods

2.1. Chemicals

Chemicals were used as received without a further purification process. They include Zinc nitrate hexahydrate (99%, Tianjin Kemiou Chemical Reagent, China), 2-methylimidazole (Hmim) (Sinopharm chemical reagent Co. Ltd., China), ammonium hydroxide solution (NH_3, 25–28%, Nanjing Chemical Reagent Co. Ltd., China), anhydrous ethanol (99.7%, Sinopharm chemical reagent Co. Ltd., China) and CV and MG were purchased (Merck KGaA, 64271 Darmstadt, Germany).

2.2. Characterization techniques

FTIR analysis was conducted using a JASCO-FT/IR-4100 spectrometer (Jasco, Easton, MD, USA): the finely grinded sample of ZIF-8 was included in the KBr discs prior to analysis in the 400–4000 cm^{-1} wavenumber range. A Shimadzu XRD-6000 diffract meter (Shimadzu Company, Tokyo, Japan) equipped with Cu Kα radiation (λ = 1.54 Å) was used to investigate structural deviations of the as-prepared ZIF-8 sample. The 2θ range was varied between 5–80° at a scanning rate of 0.02°. The values of the crystal structure, space group and lattice parameters were calculated and optimized using the computer databases CRYSFIRE and CHEKCELL. UV-visible spectrophotometer (HACH LANGE DR5000) used 1.0 cm quartz cell for sample absorbance measurement. N_2 adsorption-desorption isotherms were recorded at the bath temperature (77 K) on Quanta chrome Touch Win v1.2. Using the Brunauer-Emmett-Teller (BET) process, from which the pore volume of the BET surface and the Barrett-Joyner-Halenda (BJH) was measured. The surface morphology of MINs was analyzed

using scanning electron microscope (SEM) analysis using gold coating inspection to accelerate voltages of 20 kV (JEOL-JSM-6510 LV). The elemental distribution of MINs was studied using the energy-dispersive X-ray spectroscopy (EDX) and was taken on a 5 kV operating voltage Leo1430VP microscope. For pH adjustment HANNA instrument pH meter (model 211) was used. The instrument Maxturdy 30 (Wisd) was used for shaking at temperature level.

2.3. Preparation of the Adsorbent

According to previously published research, ZIF-8 was synthesized [11]. In a standard synthesis, 2.97 g of zinc nitrate hexahydrate ($Zn(NO_3)_2.6H_2O$) was dissolved in 3g of deionized water; 1.64 g of Hmim was added in 20.75 mL ammonium hydroxide solution; afterwards, Zinc nitrate and Hmim solutions were mixed together. The solution immediately became milk-like suspension, and stirred at room temperature for 10 min to complete the crystallization (Fig.1). The sample was collected through centrifugation and washed three times with deionized water until the final product had pH value about 7, then dried overnight at 60 °C.

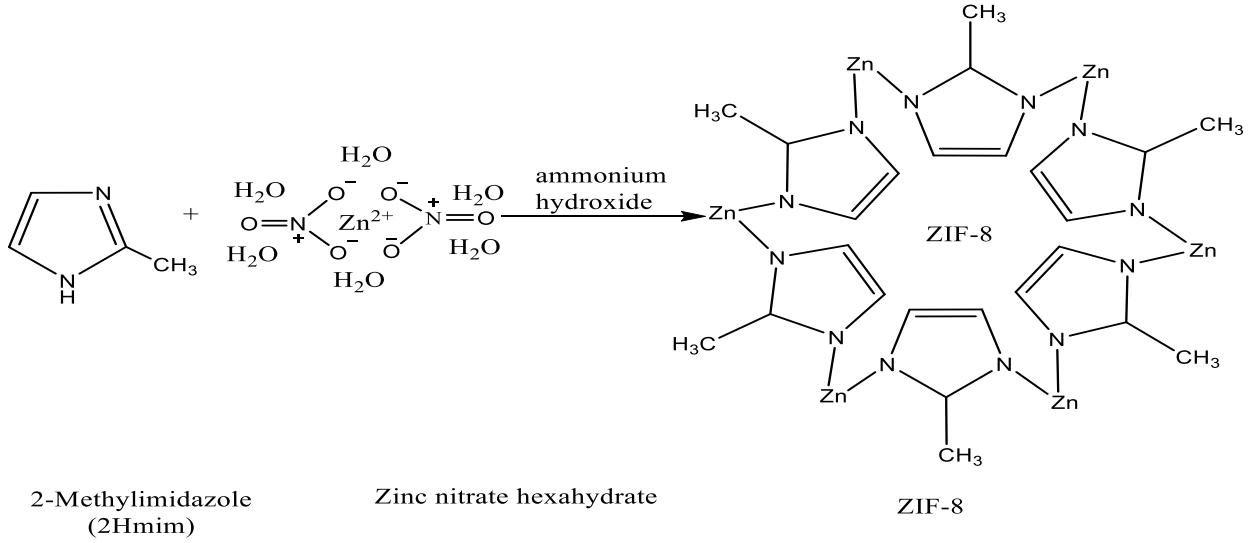

Fig.1 Synthesis of ZIF-8.

2.4. Experimental design for batch adsorption studies

A stock solution (1×10^{-3} molL^{-1}) of Crystal violet (CV) and Malachite green (MG) dye was prepared by dissolving an appropriate quantity of the powder in distilled water. The other solutions were obtained just before the experiments by diluting stock solution with distilled water [12]. For the study of the effect of pH, 25 mL of 1.9×10^{-4} and $2.5\text{x}10^{-4}$ molL^{-1} CV and MG solution, respectively, at different pH values (in the range of 2 to 10) were mixed with 20 mg of sorbent (ZIF-8) for 90 min, and the stirring speed was held at 200 rpm using a water bath for the shakers. The pH values were adjusted by addition of 0.1 or 0.01 molL^{-1} HCl, and 0.1 or 0.01 molL^{-1} NaOH solutions and measured by using a pH meter [13,14]. Samples were collected and filtered at 3000 rpm for 5 min by centrifuge separation and the filtrate was analyzed for residual dye concentration using 590 and 625 nm wavelength spectrophotometer for CV and MG, respectively. During sorption the pH was not regulated but the final pH was systematically reported. Percentage of dye removal (R) was calculated using (Eq. (1):

$$\%R = \frac{(C_0 - C_t)}{C_0}\ x\ 100 \qquad (1)$$

where C_0 (mmolg^{-1}) and C_t (mmolg^{-1}) are dye concentration initially and at time t, respectively.

For sorption isotherms, 20 mg of sorbent (ZIF-8) were mixed with 25 mL of dye solutions at different initial concentrations (C_0, ranging between 2.7x10^{-5} and 2.2x10^{-4} molL^{-1}, pH 9 for CV; and between 2.5x10^{-5} and 4.8x10^{-4} molL^{-1}, pH 8 for MG) for 90 min. After solid–liquid separation, the residual concentration (C_e, mmolL^{-1}) was determined by a UV–vis spectrophotometer and the sorption capacity (q_e, mmolg^{-1}) was determined by the mass balance equation (Eq. 2):

$$\mathbf{q_e} = \frac{(\boldsymbol{C_0 - C_e})\boldsymbol{V}}{\boldsymbol{M}} \quad (2)$$

where C_0 and C_e are the initial and equilibrium concentrations of dye in solution (mol L^{-1}), respectively, V is the volume of solution (L), and M is the mass of sorbent (g). For uptake kinetics, 120 mg of sorbent were mixed with 150 mL of dye solutions (C_0, 1.9×10^{-4} molL^{-1}, pH 9 for CV; and 2.5x10^{-4} molL^{-1}, pH 8 for MG). Samples (1 mL) were collected at fixed times (the sorbent being centrifuged separated) and the residual concentration was measured by a UV vis-spectrophotometer. The agitation speed was set at 200 rpm, and the temperature was maintained at 298 K. The sorbet amount of dye per unit weight of the sorbent at time t (q_t, mmolg^{-1}) was calculated from the mass balance equation (taking into account the decrement in the volume of the solution) as follows (Eq. 3):

$$\boldsymbol{q_{(i)}} = \sum_{\boldsymbol{i=1}}^{\boldsymbol{n}} \frac{[\boldsymbol{C(t)_{(i-1)} - C(t)_{(i)} V(t)_{(i-1)}}]}{\boldsymbol{M}} \quad (3)$$

where $C(t)_{(i)}$ (molL^{-1}) is the dye concentration of the withdrawn sample number i at time t, $C(t)_{(0)} = C_0$, $V(t)_{(i)}$ (mL) is the volume of the solution in the flask at sample number i and time t, and M is the mass of the sorbent in the flask. Here, $V(t)_{(i)} - V(t)_{(i-1)} = 1$ mL (the sample volume).

The effect of temperature on the adsorption of dye was carried out in the 25 mL of dye solutions (1.9×10^{-4} molL^{-1}, pH 9 for CV; and 2.5x10^{-4} molL^{-1}, pH 8 for MG) with 20 mg of adsorbent for 30 min at various temperatures (293, 298, 303, 308, 313, and 318 K).

The effect of sorbent dose on AR57 and RR dye removal was carried out in the 25 mL of dye solutions (1.9×10^{-4} molL^{-1}, pH 9 for CV; and 2.5x10^{-4} molL^{-1}, pH 8 for MG). with adsorbent varying from 10 to 100 mg at 298 K for 90 min [15].

The zero charge point (pH_{PZC}) was calculated by means of a solid addition process. A series of 0.1 M KNO_3 solutions (50 ML each) were prepared and their pH values were adjusted in the range of 1.0 to 12.0 by addition of 0.1 or 0.01 molL^{-1} HCl, and 0.1 or 0.01 molL^{-1} NaOH. 0.1 g of MINs was applied to each solution and the suspensions were shackled manually, and the solution was held at 293 K for duration of 48 h with occasional manual shaking. The final pH of the solution was reported and the difference was plotted against the initial pH (X-axis) between the initial and final pH (ΔpH) (Y-axis) [15].

3. Result and discussion

3.1. Characterization of ZIF-8

3.1.1 X-ray diffraction (XRD) patterns

The as-synthesized ZIF-8 pattern XRD is shown in Fig. 2. The sample may be assigned to ZIF-8, and no other phase was detected in these samples [13]. According to the XRD study in The presence of strong peaks at 2θ = 9.94, 12.29, 14.28, 15.91, 17.35 and 18.98° correspond to planes (011), (002), (112), (022), (013), and (222), respectively, which indicates high crystallinity of the prepared ZIF-8 (JCPDS 00-062-1030). The crystallite size (D, Å) of the ZIF-8 nanoparticles was calculated by using the Scherrer formula Eq. (4):

$$D = K\lambda / \beta \mathrm{Cos}\theta B \quad (4)$$

where λ is the X-ray wavelength (1.54 Å), β is the angular width of the peak at half its maximum intensity (full width at half-maximum) correctes for instrumental broadening, B is the maximum of the Bragg diffraction peak, and K is the Scherrer constant (0.9 Å). The crystallite size of ZIF-8 calculated from the high-intensity (002) peak was 355 nm [16].

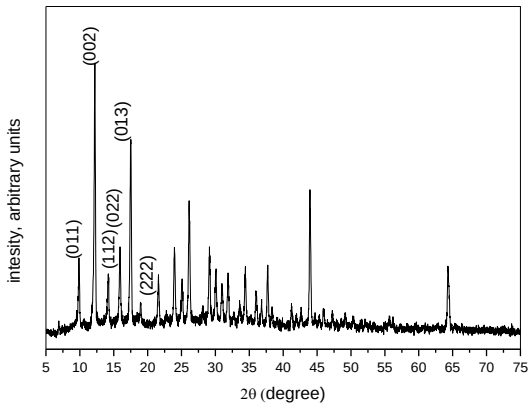

Fig. 2. XRD patterns of the as-synthesized ZIF-8 (JCPDS 00-062-1030).

3.1.2. Fourier transforms infrared (FTIR) analysis

The functional groups present in the ZIF-8 material were analyzed from the FT-IR within 4000-400 cm^{-1} range. The ZIF-8 FT-IR spectrum is given in Fig. 3. The absorption bands obtained at 2930 and 3134 cm^{-1} correspond to the imidazole stretching of the aromatic and aliphatic C–H, respectively. The deep bands at 1380–1583 cm^{-1} are consistent with the entire ring stretching. The 2-methyl imidazole absorption band at 1583 cm^{-1} can be classified as C=N stretching mode. The bands in the 952–1380 cm^{-1} spectral region is for the bending of the ring in plane. The C–N stretch has been measured in the range of 1460–1143 cm^{-1} and the 420 cm^{-1} band is assigned to the Zn–N stretch [17].

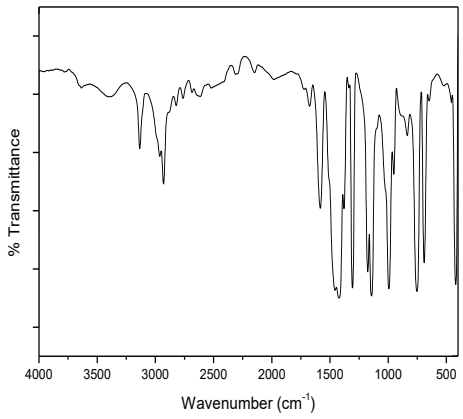

Fig. 3. FTIR spectrum of as-synthesized ZIF-8.

3.1.3. Brunauer-Emmett-Teller (BET) surface area.

The pores surface area and volume are also very important parameters to describe in a porous material as the size and volume of the pores can greatly affect the properties of the materials and the processability of the applications. It is normally done by the measurement of the substance's surface area on the Brunauer-Emmett-Teller (BET). BET measurements use an adsorption isotherm based on physisorption and a gas's propensity to become weakly bound to an external surface of materials when it comes into contact. Physisorption is a reversible process and therefore a gas can adsorb and desorb to the material surface easily. The volume of gas which is adsorbed at a set of different pressures, at constant temperature, is calculated to give the adsorption isotherm. The temperature is normally kept stable using liquid nitrogen, hence the

temperature is ~77 K. The sum of gas adsorbed by a set of different pressures that gives the graph called an adsorption isotherm. The curve form on the graph provides insight into the sort of pores that the material has Fig.4. The isothermic adsorption is graded as type I of ZIF-8. A hysteresis loop is observed at higher relative pressure ($P/P^0 > 0.9$) due to the presence of pores which are usually microporous with the exposed surface remaining almost entirely within the microspores, which once filled with adsorbents; leave little to no external surface for further adsorption. BET surface area was 495,199 m^2/g, adopting a value of 16.2 Å for the N_2 molecule's cross-sectional area. Nevertheless, the total volume of pore taken at a saturation pressure is 0.2756 cm^3/g and the average pore diameter is 2.23 nm. The surface area of BJH was 21,824 m^2/g, pore volume 0,026 cm^3/g, and pore diameter Dv(d) 3,986 nm, respectively. The volume of a micropore was 0.241 cm^3/g. The micropore area of 470.404 m^2/g and the external area of 27.795 m^2/g (calculated using t-plot method) were beneficial for the application of adsorption[18].

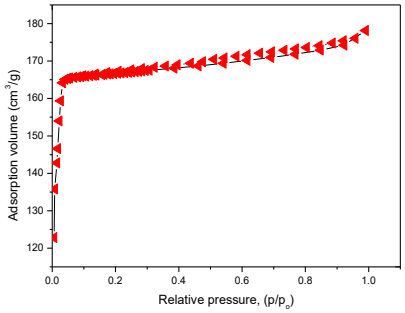

Fig. 4. N_2 adsorption/desorption isotherm of ZIF-8.

3.1.4. SEM analysis

Scanning electron microscopy (SEM) has been considered a primary method of characterizing the adsorbent structure, basic physical properties and morphology. This is useful for determining the porosity of adsorbents, the shape of particles and the appropriate size distribution. ZIF-8 SEM analysis (Fig. 5) approved ZIF-8 to be nano particles, as its average diameter ranged from 165 to 348 nm. ZIF-8 has a large number of pores in which colors can be adsorbed and trapped in these pores [19].

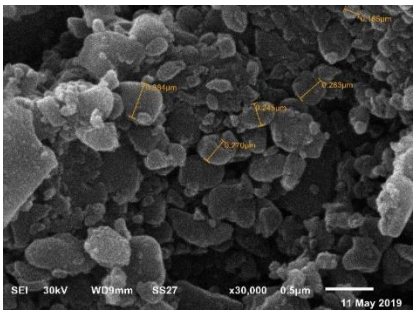

Fig.5. SEM image of ZIF-8.

3.1.5. Energy-dispersive X-ray spectroscopy (EDX)

The energy-dispersive X-ray spectroscopy (EDX) is an analytical method used mainly to demonstrate the elemental analysis or chemical composition of the sample. It is the basic idea that each element has a specific atomic structure allowing for a unique set of peaks on the EDX spectrum indicates the existence of ZIF-8.as the presence of C , N, and Zn. In closing, The EDX analysis confirms the formation of ZIF-8 and also shows that its synthesis technique is useful, since no element loss was observed during the process. [20].

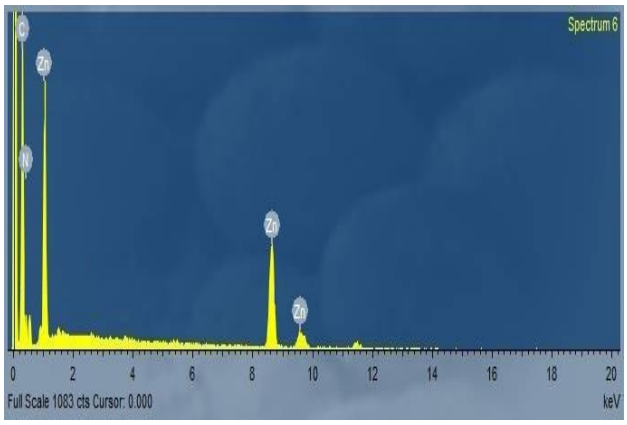

Fig.6. EDX spectrum of ZIF-8.

3.1.6. Molecular Structure

The molecular structure of the ZIF-8 was optimized by HF method with a 3-21 G basis package. Built using Perkin Elmer Chem. Carbon. Draw., Use of Perkin Elmer ChemBio3D software to optimize the molecule. The geometric parameters, bond lengths and bond angles (Table 1,2) and the molecular structure of the ZIF-8 are determined are pressented in Fig.7.

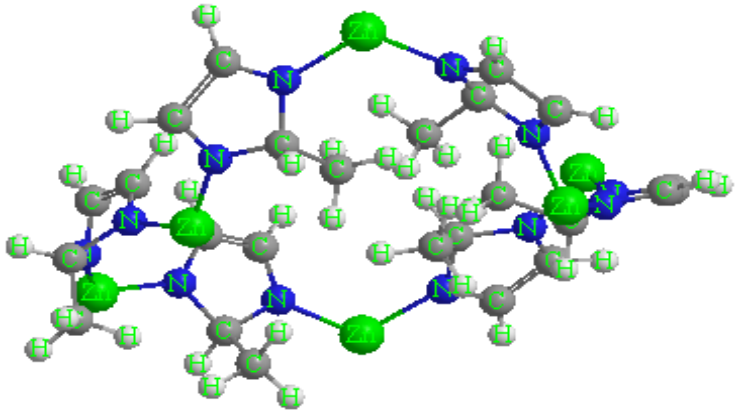

Fig.7 The calculated molecular structure of ZIF-8.

The ZIF-8 molecular structures (HOMO & LUMO) are described in Fig. 8. The HOMO – LUMO energy gap, which is an important index of stability, is used in many molecular systems to develop theoretical models to explain the barriers of structure and conformation. The lower the volume of PE, the greater the reactivity of the compound [21].

Table 3 measured quantum chemical parameters. Additional parameters such as separation energies, χ, chemical potentials, ΔE, absolute electronegativity, η, absolute softness, σ, global electrophilicity, Pi, absolute hardness, S, and additional electronic charge, ω, global softness, ΔN_{max}, were determined according to calculated according to Eqs. (5-12):

$$\Delta E = E_{LUMO} - E_{HOMO} \quad (5)$$

$$\chi = \frac{-(E_{HOMO} + E_{LUMO})}{2} \quad (6)$$

$$\eta = \frac{E_{LUMO} - E_{HOMO}}{2} \quad (7)$$

$$\sigma = 1/\eta \quad (8)$$

Table 1. The bond lengths of ZIF-8.

Bond lengths (Å)		Bond lengths (Å)		Bond lengths (Å)	
C(42)-H(78)	1.114	C(2)-H(43)	1.097	N(14)-C(15)	1.266
C(42)-H(77)	1.114	Zn(26)-N(24)	1.926	C(11)-C(13)	1.531
C(42)-H(76)	1.114	Zn(26)-N(14)	1.926	C(11)-N(7)	1.476
C(39)-H(75)	1.116	Zn(27)-N(32)	1.926	N(10)-C(11)	1.477
C(37)-H(74)	1.097	Zn(27)-N(21)	1.926	C(9)-N(10)	1.266
C(36)-H(73)	1.097	Zn(40)-N(29)	1.926	C(8)-C(9)	1.337
C(34)-H(72)	1.114	Zn(40)-N(38)	1.926	N(7)-C(8)	1.266
C(34)-H(71)	1.113	Zn(41)-N(35)	1.926	C(5)-C(6)	1.532
C(34)-H(70)	1.113	Zn(41)-N(4)	1.926	C(5)-N(1)	1.477
C(33)-H(69)	1.116	Zn(12)-N(1)	1.926	N(4)-C(5)	1.478
C(31)-H(68)	1.097	Zn(12)-N(10)	1.926	C(3)-N(4)	1.266
C(30)-H(67)	1.097	Zn(19)-N(7)	1.926	C(2)-C(3)	1.336
C(28)-H(66)	1.113	Zn(19)-N(17)	1.926	N(1)-C(2)	1.266
C(28)-H(65)	1.113	C(39)-C(42)	1.532	C(15)-C(16)	1.337
C(28)-H(64)	1.114	C(39)-N(35)	1.476	N(32)-C(33)	1.477
C(25)-H(63)	1.116	N(38)-C(39)	1.476	C(31)-N(32)	1.266
C(23)-H(62)	1.097	C(37)-N(38)	1.266	C(30)-C(31)	1.336
C(22)-H(61)	1.097	C(36)-C(37)	1.336	N(29)-C(30)	1.267
C(20)-H(60)	1.114	N(35)-C(36)	1.266	C(25)-C(28)	1.531
C(20)-H(59)	1.113	C(33)-C(34)	1.532	C(15)-H(55)	1.097

Table 2. The bond angles of Zif-8.

Bond angles (º)		Bond angles (º)		Bond angles (º)	
H(78)-C(42)-H(77)	107.913	H(78)-C(42)-H(77)	107.913	N(32)-C(33)-N(29)	102.665
H(78)-C(42)-H(76)	107.918	H(78)-C(42)-H(76)	107.918	C(33)-N(32)-C(31)	106.2
H(78)-C(42)-C(39)	110.997	H(78)-C(42)-C(39)	110.997	C(33)-N(32)-Zn(27)	126.277
H(77)-C(42)-H(76)	107.484	H(77)-C(42)-H(76)	107.484	C(31)-N(32)-Zn(27)	126.776
H(77)-C(42)-C(39)	111.178	H(77)-C(42)-C(39)	111.178	H(68)-C(31)-N(32)	121.008
H(76)-C(42)-C(39)	111.189	H(76)-C(42)-C(39)	111.189	H(68)-C(31)-C(30)	126.546
N(35)-Zn(41)-N(4)	117.893	N(35)-Zn(41)-N(4)	117.893	N(32)-C(31)-C(30)	112.445
N(38)-Zn(40)-N(29)	117.877	N(38)-Zn(40)-N(29)	117.877	H(67)-C(30)-C(31)	126.394
H(75)-C(39)-C(42)	111.664	H(75)-C(39)-C(42)	111.664	H(67)-C(30)-N(29)	120.984
H(75)-C(39)-N(38)	108.758	H(75)-C(39)-N(38)	108.758	C(31)-C(30)-N(29)	112.621
H(75)-C(39)-N(35)	108.756	H(75)-C(39)-N(35)	108.756	Zn(40)-N(29)-C(33)	126.452
C(42)-C(39)-N(38)	112.335	C(42)-C(39)-N(38)	112.335	Zn(40)-N(29)-C(30)	126.264
C(42)-C(39)-N(35)	112.329	C(42)-C(39)-N(35)	112.329	C(33)-N(29)-C(30)	106.057
N(38)-C(39)-N(35)	102.554	N(38)-C(39)-N(35)	102.554	H(66)-C(28)-H(65)	107.882
Zn(40)-N(38)-C(39)	127.031	Zn(40)-N(38)-C(39)	127.031	H(66)-C(28)-H(64)	107.978
Zn(40)-N(38)-C(37)	126.473	Zn(40)-N(38)-C(37)	126.473	H(66)-C(28)-C(25)	110.977
H(78)-C(42)-H(77)	106.264	C(39)-N(38)-C(37)	106.264	H(65)-C(28)-H(64)	107.425
H(78)-C(42)-H(76)	121.009	H(74)-C(37)-N(38)	121.009	H(65)-C(28)-C(25)	111.303
H(78)-C(42)-C(39)	126.546	H(74)-C(37)-C(36)	126.546	H(64)-C(28)-C(25)	111.114
H(77)-C(42)-H(76)	107.913	N(38)-C(37)-C(36)	112.444	N(32)-Zn(27)-N(21)	118.756

$$Pi = -\chi \quad (9)$$

$$S = \frac{1}{2\eta} \quad (10)$$

$$\omega = Pi^2 / 2\eta \quad (11)$$

$$\Delta N_{max} = -Pi/\eta \quad (12)$$

The value of ΔE for was found 0.817 eV.

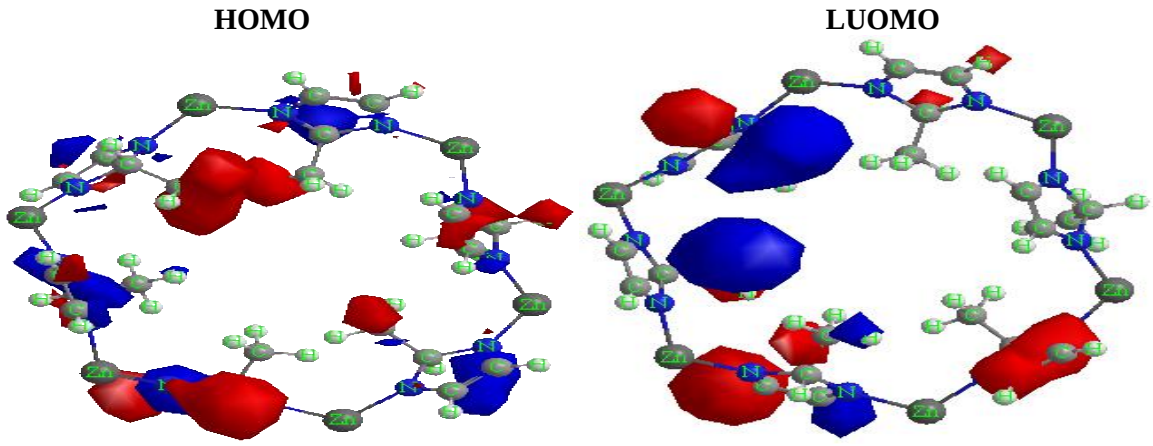

Fig. 8. The (**HOMO**) and the (**LUMO**) of ZIF-8.

Table 3. The calculated quantum chemical parameters for the investigated ZIF-8.

Compound	E_{HUMO}	E_{LUMO}	ΔE	X	η	Pi	σ	S	Ω	ΔN_{max}
	eV	eV	eV	Ev	eV	eV	eV^{-1}	eV^{-1}	eV	
ZIF-8	-3.585	-2.768	0.817	3.177	0.408	-3.18	2.45	1.22	5.05	7.78

3.2. Batch Experiments

3.2.1. Determination of point of zero charge (pH_{PZC})

PH was one of the most important parameters for sorption (CV) and (MG) as it calculated which ionic species were present in the adsorbent solution and the sorbent surface load. The PZC has determined the surface charge of the ZIF-8, which is defined as the pH (pH_{PZC}) at which the positive charges on the surface are equal to the negative charges [22]. ZIF-8 pH_{PZC} was found as 7.9 (Fig. 9). This shows that below this pH, due to protonation of functional groups, the ZIF-8 acquires a positive charge and above this pH there is negative charge on the ZIF-8 surface. cationic dyes are favored to adsorb at pH > pH_{PZC} where the surface becomes negatively charged.

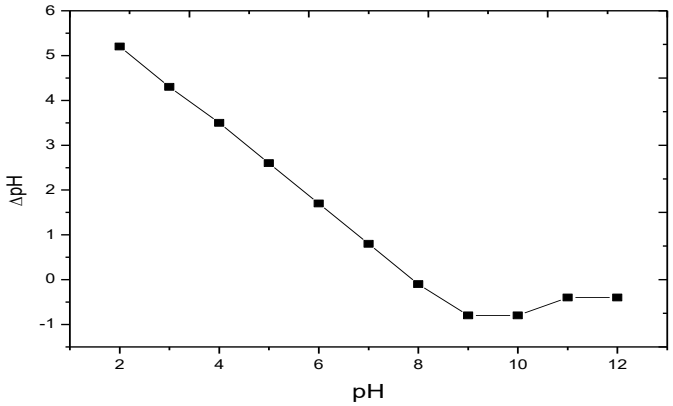

Fig. 9. Relation between initial pH and ΔpH of ZIF-8.

3.2.2. Effect of pH

Due to its effect on both the ionization of dye molecules and surface binding sites, the pH value of aqueous solution is an important parameter in the adsorption analysis of cationic colours. Deletion of the tested dyes (CV) and (MG) by ZIF-8 at different pH values (3–12) was studied at initial concentrations of $1.9x10^{-4}$ molL^{-1} of the CV, 25 °C and 0.02 g adsorbent dosage while $2.5x10^{-4}$ molL^{-1} was initial concentration of MG, 25 °C and 0.05 g adsorbent dosage. ZIF-8 It has been shown to be an effective adsorbent for removing these colors and the most effective pH was 9 for crystal violet while pH 8 for malachite green was used in further studies (Fig. 10). 10. The investigated dye was cationic in nature so on dissolution, they release colored dye cation. As the pH decreased from 8 to 2 the level of color removal decreased. For two possible adsorption mechanisms of dye on the adsorbent it may be considered: (i) electrostatic interaction between the adsorbent and the dye molecule, (ii) a chemical reaction between the dye and the adsorbent. The OH^- ion concentration increased at pH 8 and the adsorbent surface acquires negative charge by absorbing OH^- ions. Since the adsorbent surface is charged negatively at high pH, there may be a high electrostatic attraction between the adsorbent's negatively charged surface and the cationic dye molecule, maximum adsorption of the dye occurs [23].ZIF-8's experimental pH_{PZC} determination showed this composite had pH_{ZPC} 7.9. As the system's pH increases, the number of negatively charged sites is increasing, and the number of positively charged sites is falling. Thanks to the electrostatic attraction, negative charged surface sites on the adsorbent surface favored adsorption.

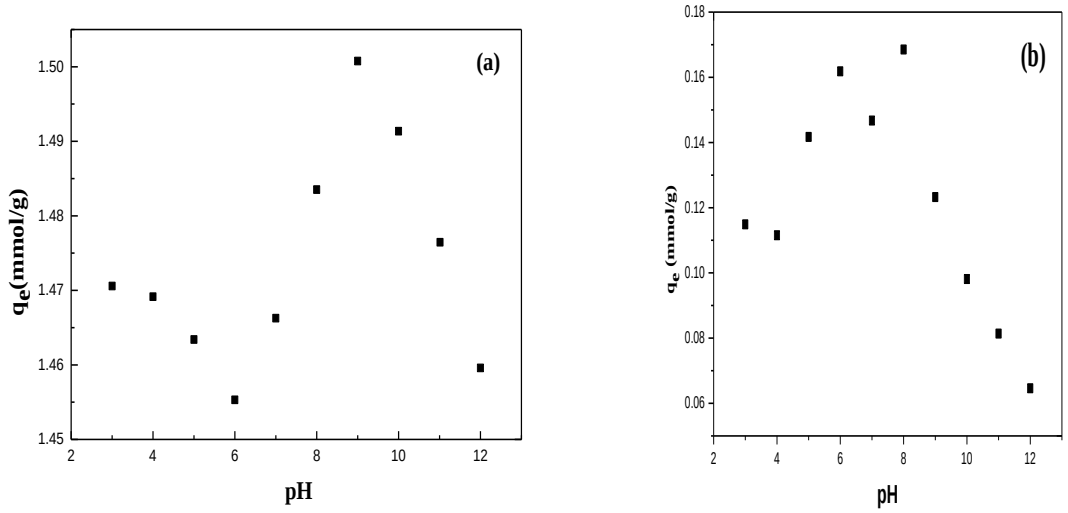

Fig. 10. (a) pH effect on CV adsorption using the adsorbent (ZIF-8): (T: 25 °C; C_0: $1.9x10^{-4}$ molL^{-1}); (b) pH effect on MG adsorption using the adsorbent (ZIF-8):(T: 25 °C; $2.5x10^{-4}$ molL^{-1}).

3.2.3. Effect of adsorbent dosage

The effect of dye removal with ZIF-8 dosage is shown in Fig. 11, Twelve. Due to the increase of adsorbent surface area and the availability of more adsorption sites against a constant amount of dye molecule it was clear that dye adsorption increased with adsorbent dosing. However, increasing the number of adsorbents causes adsorption sites to overlap or aggregate and therefore decrease in adsorption capacity takes place. The adsorption of CV and MG on the ZIF-8 sorbent was studied by changing the quantity of adsorbent range of (0.01 to 0.25) g 25 mL^{-1}, at adsorbate concentration $1.9x10^{-4}$ molL^{-1} at 25 °C and pH 9 for CV while for MG concentration $2.5x10^{-4}$ molL^{-1} at 25 °C and pH 8 was tested. The results in Fig.11a, 12a show the CV and MG adsorption capacity as a function of adsorbent amount. It has been found that the adsorption capacity decreases from 1.499 to 0.1356mmol/g mmol/g and 0.138 to 0.0596 mmol/g for CV and MG respectively. The dose of ZIF-

8 increases from 0.01 to 0.25 g 25 mL^{-1}. Fig. 11b, 12b shows the effect of dose on the equilibrium concentration (C/C_0) of CV and MG, respectively, by the ZIF-8 sorbent. As the dosage increases, the CV and MG equilibrium concentration decreases, which is due to the rise in the adsorbent surface region. The adsorbent surface is composed of active sites with a binding energy range. The ZIF-8 sorbent reveals the dose effect on the equilibrium concentration (C/C_0) of CV and MG. As the dosage increases, the CV and MG equilibrium concentration decreases, which is due to the rise in the adsorbent surface region. The adsorbent surface is composed of active sites with a binding energy spectrum. At small adsorbent dosage, all sites are fully exposed and the surface adsorption is saturated faster, with a higher adsorption efficiency. A rise in adsorbent mass contributes to a decrease in adsorption efficiency of the equilibrium per unit weight of the adsorbent (q_e) since the solution produces excess adsorbent for the small number of ZIF-8 ions. According to the result, the dose of 0.02g 25 mL^{-1} will achieve the optimum loading capacity for the sorbent, and the dose of 0.25 g 25 mL^{-1} will achieve the optimum removal efficiency. The determination of the appropriate adsorption dose therefore depends on the nature and intent of the treatment process. Therefore, if the target is the water quality norm set by WHO, a greater amount of adsorbent is better (0.25 g 25 mL^{-1}), and if the optimum loading of the sorbent per unit mass is the target, the dose of 0.02 g 25 mL^{-1} is more suitable [24].

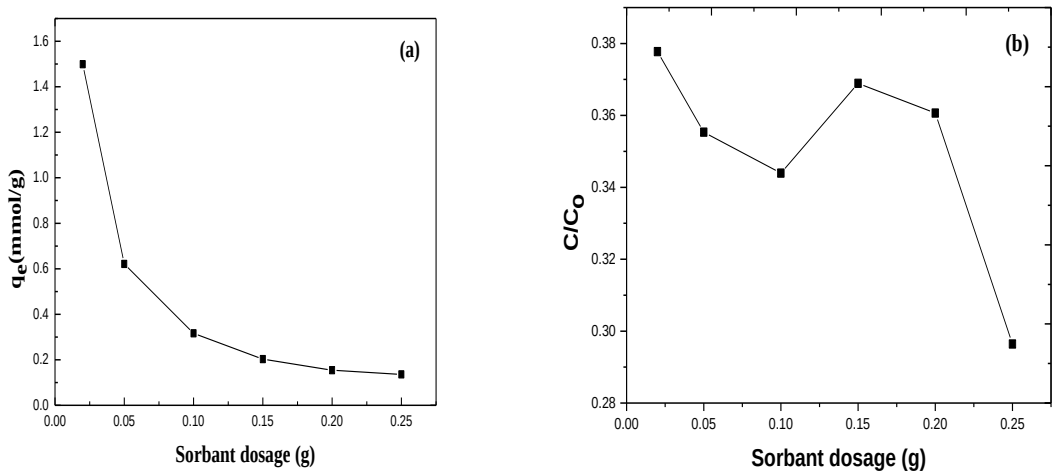

Fig. 11. Effect of ZIF-8 dosage on CV adsorption (a) Sorption capacity *vs.* SD, (b) Relative residual concentration (C/C_0) *vs.* SD (C_0: 1.9x10^{-4} $molL^{-1}$; T: 25 °C; pH 9).

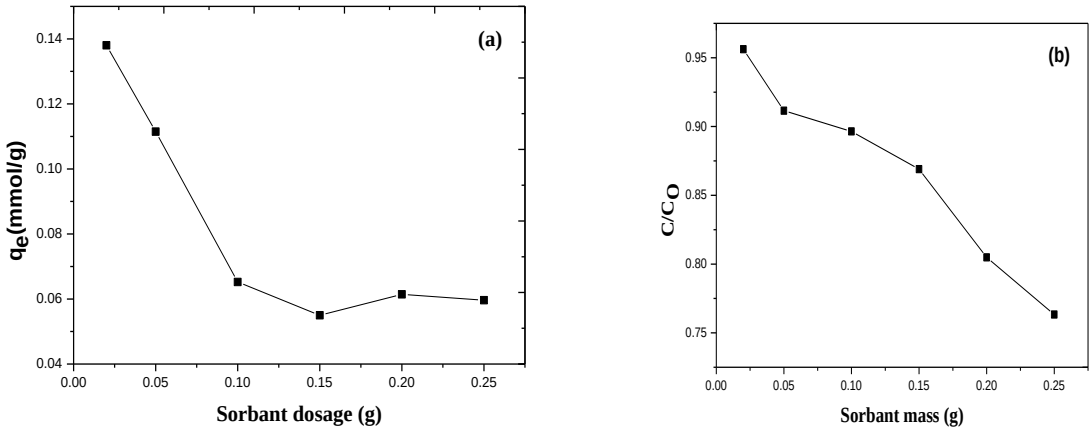

Fig. 12. Effect of ZIF-8 dosage on MG adsorption (a) Sorption capacity *vs.* SD, (b) Relative residual concentration (C/C_0) *vs.* SD (C_0: 2.5x10^{-4} $molL^{-1}$; T: 25 °C; pH 8).

3.2.4. Effect of contact time

With time, the removal of CV and MG increases and saturation reaches in around 5-100 min. The removal of adsorbate is, basically, rapid, but it decreases gradually with time until it reaches balance. During the first 60 min of adsorbent / adsorbent interaction, the dyes displayed a quick sorption rate and the rate of quantity removal becomes almost negligible due to the rapid exhaustion of the adsorption sites. The rate of removal of the volume of dye is higher in the beginning as there is a greater surface area of the adsorbent available for adsorption of the dye [25].

3.2.5. Effect initial concentration (C_0)

It was shown that the removal of CV and MG by adsorption on the adsorbent (ZIF-8) increased over time and reached a maximum value of 90 min, and then remained nearly constant. Regarding increasing the initial CV solution concentration from $2.7x10^{-5}$ to $2.2x10^{-4}$ $molL^{-1}$ at 25 °C, pH 9 and 0.02 g adsorbent dosage while $2.5x10^{-5}$ to $4.8x10^{-4}$ $molL^{-1}$ at 25 °C, pH 8 and 0.02 g adsorbent dosage for MG the amount of removed dyes was reduced. It was obvious that the removal of the color depended on the initial dye concentration, as the decrease in the initial dye concentration increased the amount of adsorbed dye [26]. This is very simple since, for a fixed adsorbent dose, the amount of active adsorption sites to accommodate adsorbent ions remains unchanged, however the adsorbent concentration rises, the adsorbent ions to be accommodated and thus the percentage of adsorption decreases. Higher removal percentage was observed at higher concentrations because of the saturation of the adsorption sites.

3.2.6. Effect of temperature

Many thermodynamic parameters are related to temperature dependence of the adsorption process. The plot of adsorbent quantity per adsorbent quantity as a function of temperature shows a slight upward trend with temperature rise from 20 to around 45 °C. The temperature of the adsorbent for a particular adsorbent will change the equilibrium capacity. In our study the experimental data obtained at pH 9 for CV solution from $1.9x10^{-4}$ $molL^{-1}$ and 0.02 g adsorbent dosage while $2.5x10^{-4}$ $molL^{-1}$, pH 8 and 0.02 g adsorbent dosage for MG show that rise in the adsorption capacity at temperature from 20 to 50 °C [27].

3.3. Adsorption isotherms

Isothermic studies provide important visions by clarifying the distribution of adsorbents between the solid and solution phases during the adsorption equilibrium, and adsorption isotherms reveal the behavior of adsorbents and how they interact with adsorbents. Equilibrium revisions which give the capacity of the adsorbent and adsorbent are described by isotherms of adsorption, which is usually the ratio between the quantity adsorbed and which remained in solution at fixed temperature at equilibrium. Numerous isothermic models were used to consider balancing adsorption of compounds from solutions such as Langmuir [28, 29] Freundlich [30], Dubinin–Radushkevich [31] and Temkin [32]. The isothermic Langmuir model embraces the uniform adsorption energies onto the adsorbent surface. It is based on the statement that monolayer adsorption is present on a completely homogeneous surface with a fixed number of identical sites and negligible interaction between adsorbed molecules [29]. The Freundlich model is an empirical equation based on the adsorption of varied affinities supporting sites of heterogeneous surface or surface. It is presumed that the stronger binding sites are first occupied, and that the binding strength decreases with the increasing occupancy of the site. [25].

Table 4. Isotherms and their linear forms for the adsorption of CV onto ZIF-8.

Isotherm	Equation		Value of parameters	
Langmuir	$\frac{C_e}{q_e} = \frac{1}{q_m K_L} + \frac{C_e}{q_m}$	The constants q_m and K_l are calculated by the plot of C_e/q_e *vs.* C_e with slope $1/q_m$ and intercept $1/(q_m K_L)$	$q_{m\ exp}$ ($mmolg^{-1}$)	1.5779
			q_m ($mmolg^{-1}$)	1.5814
			K_L ($Lmmol^{-1}$)	72186.073
			R^2	0.9999
Freundlich	$\ln q_e = \ln K_F + \frac{1}{n} \ln C_e$	K_F and n can be calculated from a linear plot of ln q_e *vs.* ln C_e	n	4.48732
			K_F ($mmolg^{-1}$)($Lmmol^{-1}$)$^{1/n}$	1.244
			R^2	0.713
Dubinin–Radushkevich	$\ln q_e = \ln Q_{DR} - K_{DR}\varepsilon^2$	The slope of the plot of ln q_e *vs.* ε^2 gives K_{DR} (mol^2/kJ^2) and the intercept yields the adsorption capacity, Q_{DR} (mmol/g)	Q_{DR}	1.17199
			K_{DR}(J^2mol^{-2})	-1.919E-09
			Ea($kJmol^{-1}$)	16.14
			R^2	0.8738
Temkin	$q_e = \beta_T \ln K_T + \beta_T \ln C_e$	The parameters β and K_T are the Temkin constants that can be determined by the plot of q_e *vs.* ln C_e	b_T($Lmol^{-1}$)	11605.096
			A_T ($kJmol^{-1}$)	14.96
			R^2	0.92487

Table 5. Isotherms and their linear forms for the adsorption of MG onto ZIF-8.

Isotherm	Equation		Value of parameters	
Langmuir	$\frac{C_e}{q_e} = \frac{1}{q_m K_L} + \frac{C_e}{q_m}$	The constants q_m and K_l are calculated by the plot of C_e/q_e *vs.* C_e with slope $1/q_m$ and intercept $1/(q_m K_L)$	$q_{m\ exp}$ ($mmolg^{-1}$)	0.16517
			q_m ($mmolg^{-1}$)	0.166
			K_L ($Lmmol^{-1}$)	10737.5
			R^2	0.99952
Freundlich	$\ln q_e = \ln K_F + \frac{1}{n} \ln C_e$	K_F and n can be calculated from a linear plot of ln q_e *vs.* ln C_e	n	9.6219
			K_F ($mmolg^{-1}$)($Lmmol^{-1}$)$^{1/n}$	0.296
			R^2	0.77376
Dubinin–Radushkevich	$\ln q_e = \ln Q_{DR} - K_{DR}\varepsilon^2$	The slope of the plot of ln q_e *vs.* ε^2 gives K_{DR} (mol^2/kJ^2) and the intercept yields the adsorption capacity, Q_{DR} (mmol/g)	Q_{DR}	-1.04456
			K_{DR}(J^2mol^{-2})	-1.277E09
			Ea($kJmol^{-1}$)	19.79
			R^2	0.8747
Temkin	$q_e = \beta_T \ln K_T + \beta_T \ln C_e$	The parameters β and K_T are the Temkin constants that can be determined by the plot of q_e *vs.* ln C_e	b_T($Lmol^{-1}$)	172532.9
			A_T ($kJmol^{-1}$)	17.0717
			R^2	0.8537

Dubinin – Radushkevich isotherm is an empirical model initially for the adsorption of subcritical vapors following a pore-filling process on microporic solids. It is used to differentiate between physical and chemical adsorption to detach a molecule from its position in the sorption space to the infinity [31]. The Temkin isotherm assumes that the adsorption heat of all molecules in the process decreases linearly when the substrate is covered and that the adsorption has a maximum uniform bond energy distribution [32]. It was found that the Langmuir isotherm model is the most appropriate model to characterize the isotherm for adsorption of both CV and MG dyes into the ZIF-8 sorbent Fig. 13 & 14. From the isothermic fitting however, the experimental data points deviated from the Freundlich lines. The isothermic fitting was plotted using the model constant parameters obtained from the linear equation plot analysis, based on the nonlinear equations. The Langmuir model introduced the strong coefficient of correlation R^2 = 0.9999 for CV and MG was 0.99952. Additionally, the q_m calculated from the isotherm Langmuir was close to the qmax experiment. Examination of the isotherm parameters suggested by Dubinin-Radushkevich for both CV and MG is determined (Table 8,9). This isotherm was developed in light of the effect of the sorbent's porous structure and the energy involved in the sorption process. The findings of the isotherm Dubinin-Radushkevich are shown in Table 6 and Fig. 16. For CV, for Table 7 and for Fig. 17 for MG. The mean energy value of sorption is 16.14 kJ.mol^{-1}, for CV and MG 19.79 kJ.mol^{-1}, respectively: this is dependable with the proposed mechanism of chemisorption. It is postulated that the vlaue 8 kJ.mol^{-1} is generally admitted to be the limit energy for distinguishing, physical (below 8 kJ.mol^{-1}) and chemical sorption (up 8 kJ.mol^{-1}). A comparison of the correlation coefficient values obtained from the isothermal models Langmuir, Freundlich, Dubinin-Radushkevich and Temkin (Tables 6,7) shows that the correlation coefficients for Langmuir isotherm are higher than those for the isothermal models Freundlich, Dubinin-Radushkevich and Temkin. This result suggests that the binding of dye ions on the surface of the sorbent may occur as a monolayer and that the absorption occurs by monolayer sorption on a homogenous surface. That should be tested for validation by experimental observation. The presence of the same type of functional groups is consoling the homogeneous surface hypothesis (or homogeneous sorption energies). The arrangement of the models according to its R^2 as follow: Langmuir> Temkin > Dubinin-Radushkevich > Freundlich for CV while for MG: Langmuir > Dubinin-Radushkevich > Temkin > Freundlich.

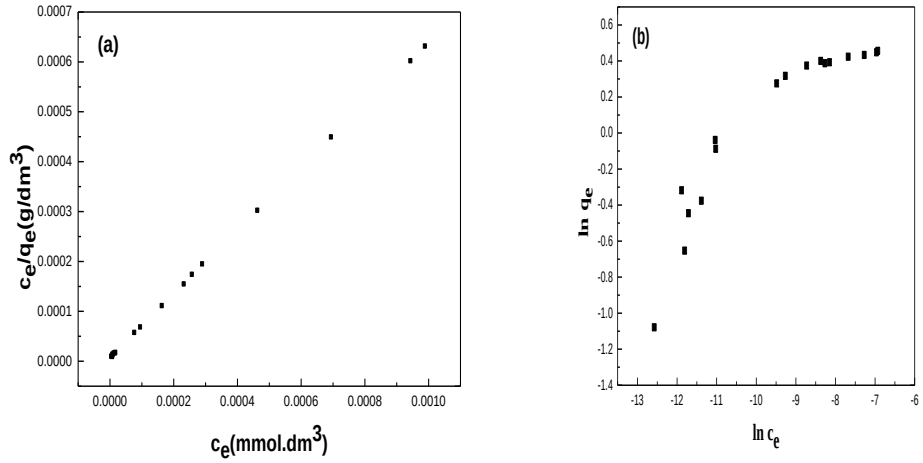

Fig. 13. Linearized plots for sorption isotherms for CV: (a) Langmuir equation, (b) Freundlich equation.

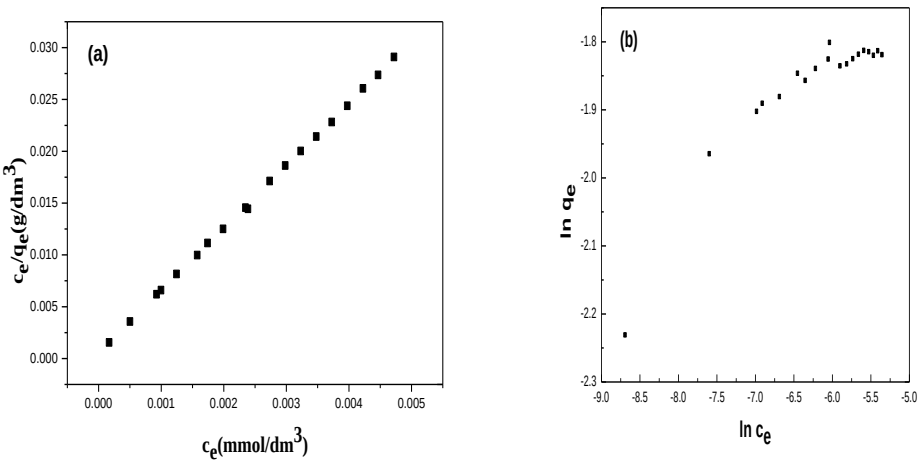

Fig. 14. Linearized plots for sorption isotherms for MG: (a) Langmuir equation, (b) Freundlich equation.

3.4. Adsorption kinetics and mechanism studies

The adsorption kinetics study describes the rate of solute uptake and this rate evidently controls the residence time of adsorbate uptake at the interface of the solid solution. The rate of removal of tested dye by adsorption was initially rapid, and then gradually slowed down until it reached an equilibrium beyond which the rate of removal was significantly increased. The highest possible adsorption was observed at 140 min. And thus the equilibrium time is set. According to the kinetic model equations below, the pseudo-first - order and pseudo-second-order kinetic models were used to determine the adsorption kinetics of tested dyes onto ZIF-8 to match the experimental results.

The pseudo-first-order Lagergren expression [33] is given as Eq. (13):

$$\log (q_e - q_t) = \log q_e - k_1 t \quad (13)$$

The pseudo-second-order kinetic model [34] is expressed as Eq. (14)::

$$t/q_t = 1/k_2 q_2^2 + 1/q_2\, t \quad (14)$$

Where q_t is an adsorbent dye (mg.g^{-1}) at various times t, q_e is the maximum adsorption capacity (mg.g^{-1}) for pseudo-first - order adsorption, k_1 is the pseudo-first - order adsorption constant (min−1), q_2 is the maximum adsorption capacity (mg.g^{-1}) for pseudo-second - order adsorption, The k_2 is the pseudo-second - order adsorption rate constant (gmg^{-1}min^{-1}). For the pseudo-first - order reaction, the straight-line log plots ($q_e - q_t$) *vs*. t and the pseudo-second - order reaction t/q_t *vs*. t Fig. 16,17. The rate parameters were also measured for the adsorption of measured dyes onto (ZIF-8). The k_1, k_2, q_e, q_2, and correlation coefficients, R_1^2 and R_2^2 for the dye were determined from these plots and are given in Table 6,7.

Table 6. Kinetic parameters and their correlation coefficients for the adsorption of CV onto ZIF-8.

Model	Equation		Value of parameters	
Pseudo-First-order kinetic	$\log(q_e - q_t) = \log q_e - \left(\frac{K_1}{2.303}\right)t$	The plot of ln (q_e - q_t) against t gives a straight line with the slope -K_1 and intercept ln q_e	K_1 (min^{-1})	-0.0144
			q_e ($mmolg^{-1}$)	0.12885
			R^2	0.88588
Pseudo-second-order kinetic	$\frac{t}{q_t} = \frac{1}{K_2 q_e^2} + \frac{t}{q_e}$	Values of K_2 and q_e for different initial concentrations of dye were calculated from the slope and intercept of the linear plot of t/q_t *vs.* t	K_2 ($g\ mg^{-1}\ min^{-1}$)	0.477799
			q_e ($mmolg^{-1}$)	1.5747
			R^2	0.99975
Intraparticle diffusion	$q_t = K_i\, t^{1/2} + X$	The parameters K_{dif} and C were determined from the linear plot of q_t *vs.* $t^{1/2}$	K_i ($mgg^{-1}min^{1/2}$)	0.00517
			X (mgg^{-1})	0.06414
			R^2	0.92685
Elovich	$q_t = \frac{1}{\beta}\ln(\alpha\beta) + \frac{1}{\beta}\, lnt$	The constants α and β were obtained from the slope and intercept of a line plot of q_t *vs.* ln t	β (g/mg)	-168.067
			α ($mgg^{-1}.min^{-1}$)	1.0507
			R^2	0.25347
Experimental data			q_e (exp) ($mmolg^{-1}$)	1.5779

Table 7. Kinetic parameters and their correlation coefficients for the adsorption of MG onto ZIF-8.

Model	Equation		Value of parameters	
Pseudo-First-order kinetic	$\log(q_e - q_t) = \log q_e - \left(\frac{K_1}{2.303}\right)t$	The plot of ln (q_e - q_t) against t gives a straight line with the slope -K_1 and intercept ln q_e	K_1 (min^{-1})	-0.01708
			q_e ($mmolg^{-1}$)	0.033889
			R^2	0.88684
Pseudo-second-order kinetic	$\frac{t}{q_t} = \frac{1}{K_2 q_e^2} + \frac{t}{q_e}$	Values of K_2 and q_e for different initial concentrations of dye were calculated from the slope and intercept of the linear plot of t/q_t *vs.* t	K_2 ($g\ mg^{-1}\ min^{-1}$)	0.995798
			q_e ($mmolg^{-1}$)	0.173
			R^2	0.99812
Intraparticle diffusion	$q_t = K_i\, t^{1/2} + X$	The parameters K_{dif} and C were determined from the linear plot of q_t *vs.* $t^{1/2}$	K_i ($mgg^{-1}min^{1/2}$)	-0.00595
			X (mgg^{-1})	0.04943
			R^2	0.25347
Elovich	$q_t = \frac{1}{\beta}\ln(\alpha\beta) + \frac{1}{\beta}\, lnt$	The constants α and β were obtained from the slope and intercept of a line plot of q_t *vs.* ln t	β (g/mg)	-48.19
			α ($mgg^{-1}.min^{-1}$)	1.08949
			R^2	0.41888
Experimental data			q_e (exp) ($mmolg^{-1}$)	0.16517

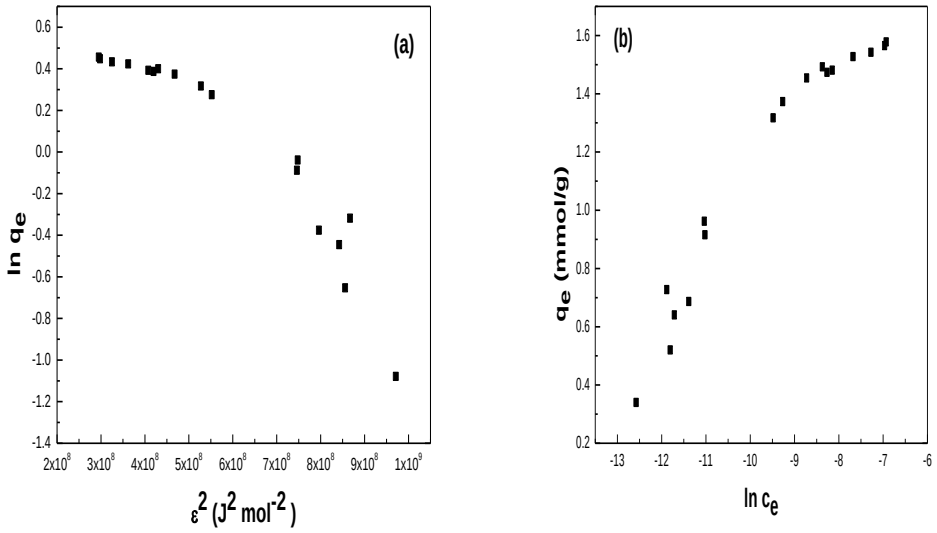

Fig. 16. Linearized plots for sorption isotherms for CV: (a) Dubinin–Radushkevich equation, (b) Temkin model.

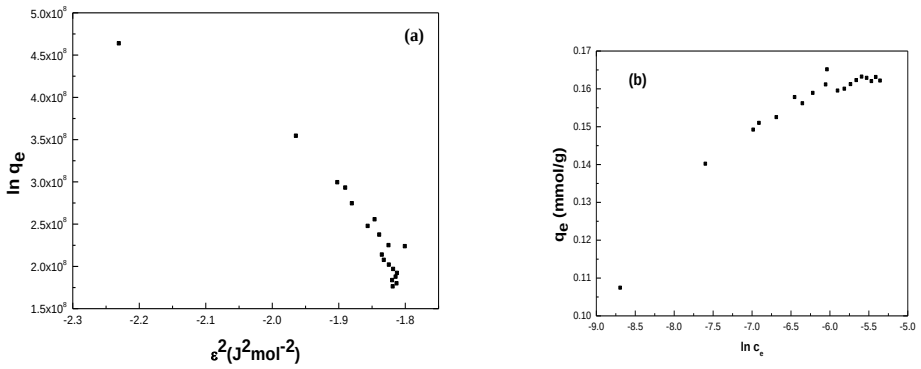

Fig. 17. Linearized plots for sorption isotherms for MG: (a) Dubinin–Radushkevich equation, (b) Temkin model.

Since the diffusion mechanism cannot be described by either the pseudo-first-order or the pseudo-second - order model, the kinetic results were further analyzed for diffusion mechanism by using the intra-particle diffusion model. The effect on adsorption of the constant intraparticle diffusion (internal surface and pore diffusion) can be calculated by the following Eq. (15).

$q_t = k_{id} t^{1/2} + I$ (15)

Where I am the interceptor and the k_{id} is the intraparticle diffusion rate constant (mg g^{-1} $min^{1/2}$) which is measureed from the linear plot of q_t *vs.* $t^{1/2}$ (Figs. 18,19), and it is commonly used to compare rates of mass transfer. According to this model, the plot of uptake, q_t, *vs.* the square root of time, $t^{1/2}$ should be linear if intra-particle diffusion is involved in the process of adsorption and if those lines move through the origin, then intra-particle diffusion is the step of power. The constant and intercept values of the intraparticle diffusion rate are shown in (Tables 8,9). The Elovich equation is used for general chemical adsorption applications [35]. The equation was successfully applied to several chemical adsorption processes and was found to cover a wide variety of sluggish adsorption levels [36]. The same equation is also valid and formulated for systems where the adsorbent surface is heterogeneous as Eq. (16):

$q_t = (1/\beta) \ln (\alpha\beta) + (1/\beta) \ln t$ (16)

Where α is the chemical adsorption rate (mg / mg min) and β is a coefficient of chemical adsorption (g/mg) in relation to the extension of covered surface and the activation energy. The qt *vs*. ln t plot gave a linear relation to the slope of (1/β) and the intercept of (1/β) ln (αβ). The 1/β value represents the number of adsorption sites available while the value of (1/β) ln (αβ) represents the adsorption quantity when ln t equal to zero.

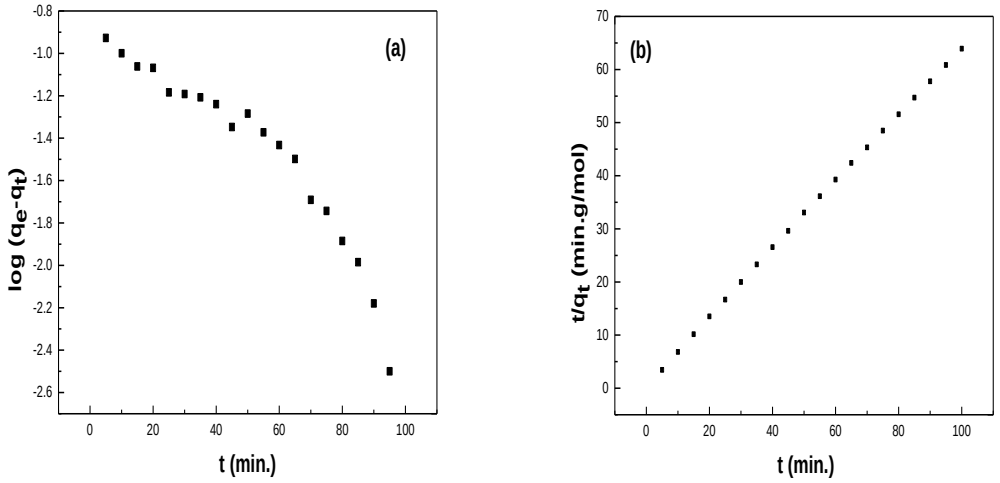

Fig. 18. Modeling of uptake kinetics for CV with: (a) pseudo-first-order rate expression, (b) pseudo-second-order rate expression.

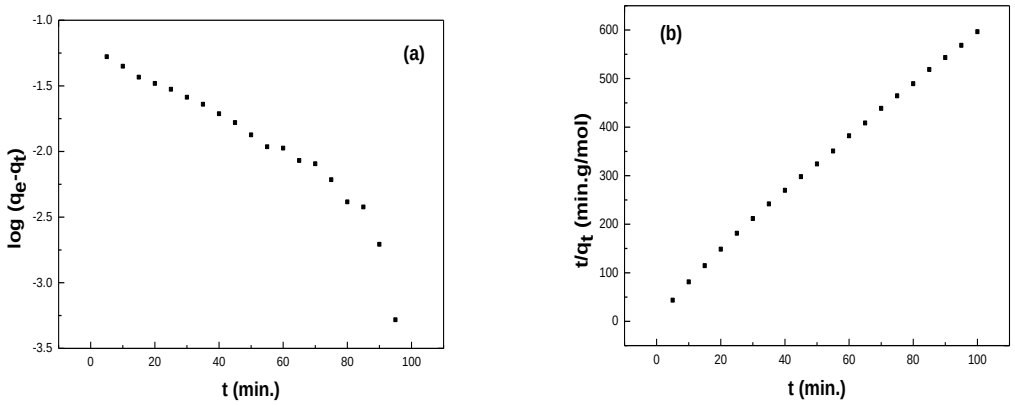

Fig. 19. Modeling of uptake kinetics for MG with: (a) pseudo-first-order rate expression, (b) pseudo-second-order rate expression.

Comparing the kinetic models, the R^2 values of the pseudo-second-order kinetic model (0.99975) are slightly higher than those of the pseudo-first-order kinetic model (0.8859) for CV, while the R^2 values of the pseudo-second - order kinetic model (0.99812) for MG are far higher than those of the pseudo-first-order kinetic model (0.8868), Implying that the kinetics of adsorption of both dyes follow the pseudo-second order kinetic model. The correlation coefficients confirm this consideration, and the value of q_e (calc.) from the pseudo-second-order kinetic model is in good agreement with the experimental results. In this adsorption process, the rate-limiting step may be chemisorption involving strong forces through sharing or Exchange of electrons from sorbent to sorbate [22]. Multilinearity is provided by the intra-particle diffusion curve; it does not pass through the origin. The kinetic intraparticle diffusion model (R^2 = 0.92685 and 0.25347) for CV and MG was determined from the slope of the corresponding second linear area (Figs. 20,21). The external resistance to the mass transfer surrounding the particles is assumed to be only significant in the initial stages of adsorption (initial sharp rise). The second linear portion is the phase of gradual adsorption, with intraparticle diffusion

control. If the plots do not pass through the origin, indicates that the diffusion of the pore is not the only rate limiting step But other kinetic models may also regulate the adsorption rate, all of which may work at the same time [37]. The Elovich equation assumes that the adsorbent's active sites are heterogeneous, and thus exhibit various chemisorption activation energies. When the dye concentration increased, it was observed that the constant α (regarding the rate of chemisorption, the β constant (related to surface coverage) increased and decreased Tables 6,7 This is due to a drop in the adsorption surface usable for adsorbents. Thus, by increasing the concentration, the rate of chemisorption may be increased within the range studied [38]. Therefore, the adsorption kinetics can be approximated satisfactorily by the pseudo-second - order kinetic model, on the assumption that the rate-limiting step may be chemisorption involving electrostatic forces through the sharing or exchange of electrons between the adsorbent and the adsorbent. The adsorption mechanism may be explained by the electrostatic interactions between the positively charged dye ion on the ZIF-8 surface and the negatively charged sites. CV and MG contain cationic dyes (N^+). The dye is dissociated to the chloride anion (Cl^-) and nitrogen ion (N^+) in aqueous solution. The nitrogen ions may bind to the group (OH^-) at base pH. However, in a strong alkaline environment, ZIF-8 showed high adsorption capacity for both CV and MG. The increased efficiency in a heavy alkaline environment resulted from the higher charged ZIF-8 (pH > pHpzc) and the increased yield of OH^- facilitated by increased concentration of OH^-. The results showed that ZIF-8 can be applied to adsorb cationic dye as a highly efficient Adsorbent.

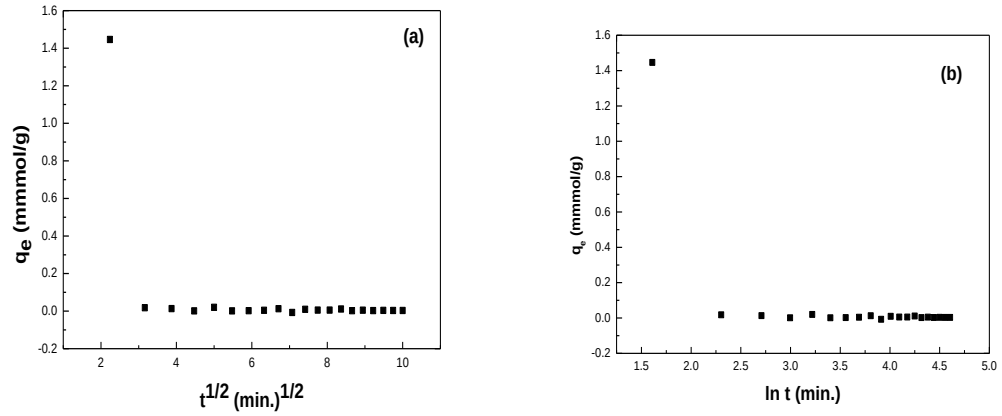

Fig. 20. Modeling of uptake kinetics for CV with (a) simplified model of resistance to intraparticle diffusion (Morris and Weber equation), (b) Elovich equation.

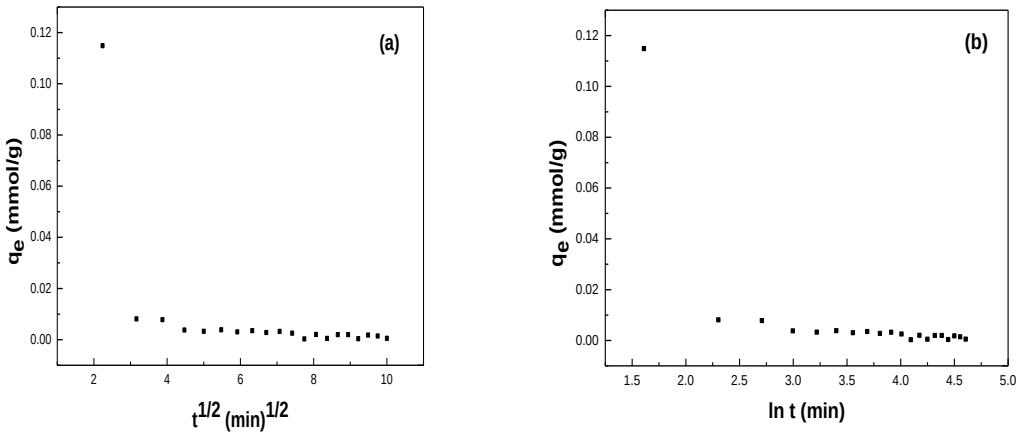

Fig. 21. Modeling of uptake kinetics for MG with (a) simplified model of resistance to intraparticle diffusion (Morris and Weber equation), (b) Elovich equation.

3.5. Thermodynamic parameters

In the light of practical application, it is important to investigate the effect of temperature on adsorption. The experiments on adsorption were conducted at five different temperatures including 20, 25, 30, 35 and 45 °C. The adsorption potential increases marginally from 0.961 to 0.9817 mmol.g^{-1} for CV and from 1.39 to 1.997 for MG, with temperature rise from 20 to 45 °C. That conduct confirms that The CV and MG adsorption onto ZIF-8 is endothermic. This discovery can be due to an increase in the mobility of coloring molecules and the rate of diffusion of adsorbent molecules across the adsorbent surface with increased temperature, resulting in an increase in adsorption capability [39, 40]. The adsorption equilibrium constant, Kc was determined (Eq. 17) and used for the evaluation of the thermodynamic constants of the sorbents with the van't Hoff equation (Eqs.18,19) and conventional thermodynamic equation (Eq. 20). (i.e., the standard enthalpy change, ΔH^o, the standard free Gibbs energy, ΔG^o, and the standard entropy change ΔS^o).

$$K_c = \frac{q_e}{C_e} \qquad (17)$$

Where q_e and C_e are the equilibrium concentration of CV and MG of the adsorbent and in solution, respectively.

$$\Delta G^o = - RT \ln K_c \qquad (18)$$

$$\Delta G^o = \Delta H^o - T\Delta S^o \qquad (19)$$

Therefore the van't Hoff equation becomes:

$$\ln K_C = \frac{-\Delta H^\circ}{RT} + \frac{\Delta S^\circ}{R} \qquad (20)$$

The value of standard enthalpy change (ΔH^o) and standard entropy change (ΔS^o) for the adsorption process are thus determined from the slope and intercept of the plot of $\ln K_c$ *vs.* 1/T (Fig. 22):

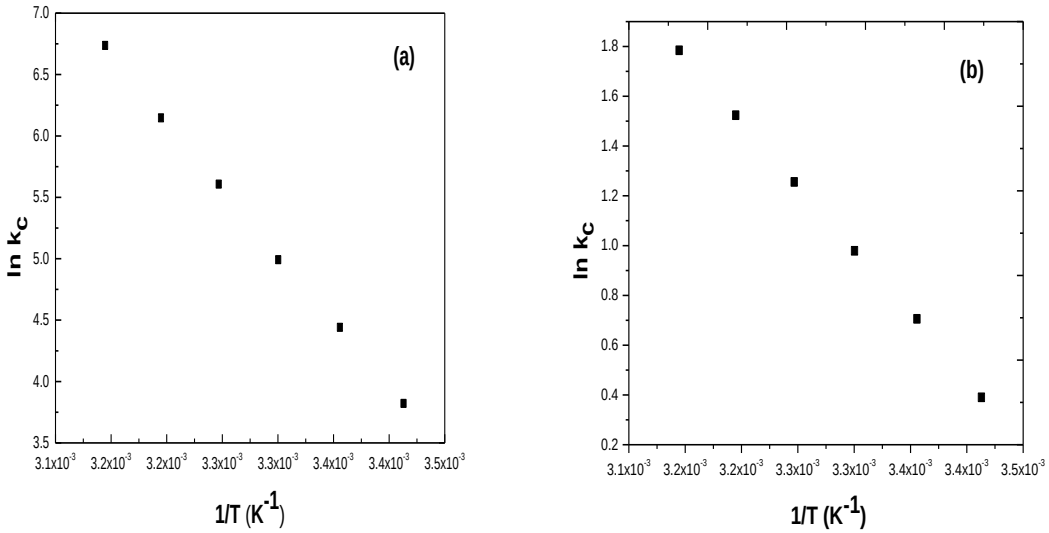

Fig. 22. (a) Van't Hoff plots for CV adsorption onto the ZIF-8 adsorbent.
(b) Van't Hoff plots for MG adsorption onto the ZIF-8 adsorbent

Table 8 shows the values of the thermodynamic parameters. The positive value of ΔH^o confirms the adsorption process's endothermic nature. ΔG^o negative values indicate spontaneous adsorption reaction. With increasing temperature, the increase in the negativity of ΔG^o confirms that the "favorability" increases with temperature. On the other hand, the positive value of the entropy change (ΔS^o) means that after dye adsorption the system's "disorder" increases [41-43].

Table 8: Standard enthalpy, entropy and free energy changes for CV and MG adsorption on ZIF-8.

	ΔH^o	ΔS^o	T_0	ΔG^o (kJ mol^{-1})					
Dye	(kJ mol^{-1})	(J mol^{-1}K^{-1})	(K)	293 K	298 K	303 K	308 K	318 K	318 K
CV	89.899	338.46	265.61	-9.26	-10.96	-12.56	-14.35	-16.0	-17.73
MG	42.97	149.97	286.54	-0.96	-1.72	-2.47	-3.22	-3.97	-4.72

3.6. Effect of ionic strength (addition of NaCl)

The effect of chloride ions on the removal of crystal violet and malachite green was examined, by adding increased NaCl concentrations (from 10 to 40 gL^{-1}; C_0: 1.9x10^{-4} molL^{-1}; sorbent dosage: 0.02 g 25 mL) for Crystal violet while for malachite green C_0: 2.5x10^{-4} molL^{-1}; sorbent dosage: 0.02 g 25 mL) (Figs. 23,24). Increasing the amount of NaCl decreases the sorption capacity slightly for the studied adsorbents: the sorption capacity decreases by about 20 percent, when the concentration of NaCl reaches 20 gL^{-1}. This is probably due to the effect of chloride anions competing against MG and CV anions for interaction with the sites of sorption. It is noteworthy that even if the concentration of NaCl reaches 40 gL^{-1} the reduction is in the adsorption capacity decreases by 1.5%, this indicates that a high adsorption capacity is maintained even under these drastic conditions. [44].

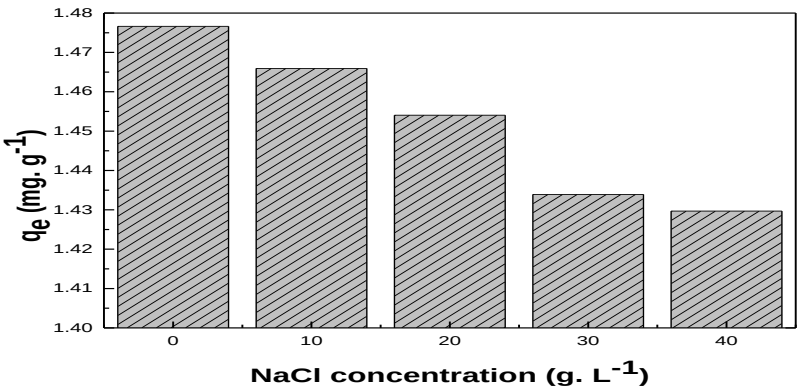

Fig. 23: Influence of NaCl on CV adsorption onto the ZIF-8 adsorbent (C_0: 1.9x10^{-4} molL^{-1}; initial pH 9; T: 25 °C; sorbent dosage: 0.02 g 25 mL^{-1}).

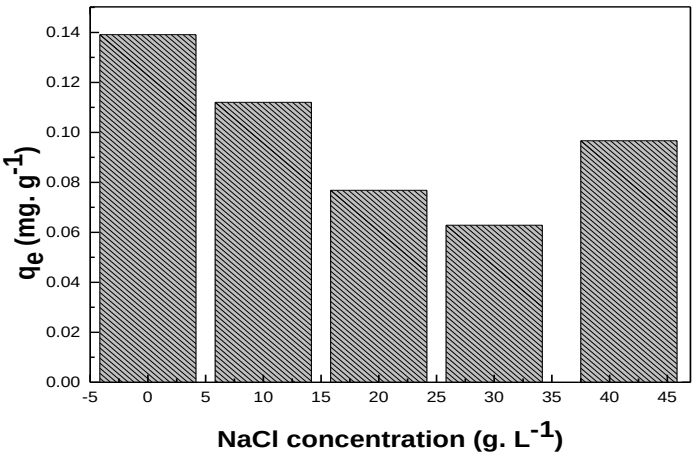

Fig. 24: Influence of NaCl on MG adsorption onto the ZIF-8 adsorbent (C_0: 2.5x10^{-4} molL^{-1}; initial pH 8; T: 25 °C; sorbent dosage: 0.02 g 25 mL^{-1}).

3.7. Comparison with other adsorbents

Comparison was made and presented in Tables 9,10 of the maximum CV and MG adsorption capacities using ZIF-8 as adsorbent with that of other adsorbents previously reported. It shows that the ZIF-8 developed possesses high CV and MG adsorption capacity.

Table 9: Adsorption capacity (q_m) of various adsorbents for the CV dye.

Adsorbent	q_m ($mg.g^{-1}$)	Reference
Tomato plant root	94.3	[45]
Sulphuric acid activated carbon	85.8	[46]
Skin almond waste	85.47	[47]
Treated ginger waste	64.9	[48]
Activated rice husk	64.87	[49]
Phosphoric acid activated carbon	60.4	[50]
Pinus bark powder	32.8	[51]
Jute fiber carbon	27.99	[52]
Wood apple	19.8	[53]
De-oil soya	5.79	[54]
Sugarcane dust	3.8	[55]
Neem sawdust	3.8	[56]
Palm kernal fiber	78.9	[57]
Potato peel	555	[58]
ZIF-8	643.78	This work

Table 10: Adsorption capacity (q_m) of various adsorbents for the MG dye.

Adsorbent	q_m ($mg.g^{-1}$)	Reference
Activated carbon was synthesized from coconut coir	27.44	[59]
SWCNT-COOH	19.84	[60]
Iron humate	19.2	[61]
Cadmium hydroxide nanowires loaded on activated carbon	19	[62]
MWCNT-COOH	11.73	[63]
SWCNTs	4.928	[62]
SWCNT-NH_2	6.134	[57]
Activated carbons commercial grade (ACC)	8.27	[60]
Bentonite clay	7.716	[64]
Activated charcoal	0.179	[65]
ZIF-8	60.27	This work

3.8. Reusability test of adsorbent

For practical applications the reusability of any porous materials such as MOFs is an important property. We have now compared ZIF-8's adsorption capacity to three consecutive cycles of adsorption-desorption. Cationic dyes are generally desorbed by a change in pH. Desorption is conducted under standard conditions in most situations. Regeneration of the investigated sorbent ZIF-8 (the adsorbent loaded with crystal violet and malachite green) was carried out by placing 0.02 g of it in the flask and then carefully washed by flowing several times using 0.01 M HCl until pH reaches 7, then wash with distilled water several times. After that the remaining amount of ethanol coloring was extracted, collect the adsorbent and put it in the oven at 60 °C for 4 hours. The adsorbent ready for second take-up after regeneration [66]. For increasing adsorption / desorption process the regeneration efficiency was found 98.6, 94.5, 69.6 %. For MG while for CV 96.7, 94.2, 62.8 %. This could be due to blockage of ZIF-8 adsorption sites. After three cycles testing we also characterized XRD of the ZIF-8 material and found that the crystallinity and structure remained intact Fig.24. This result shows the ZIF-8 has good characteristic of reusability

The efficiency of regeneration was calculated using the following Eq. (22):

$$\text{Regeneration efficiency } (\%) = \frac{\text{Total adsorption capacity in the second run}}{\text{Total adsorption capacity in the first run}} \times 100 \quad (22)$$

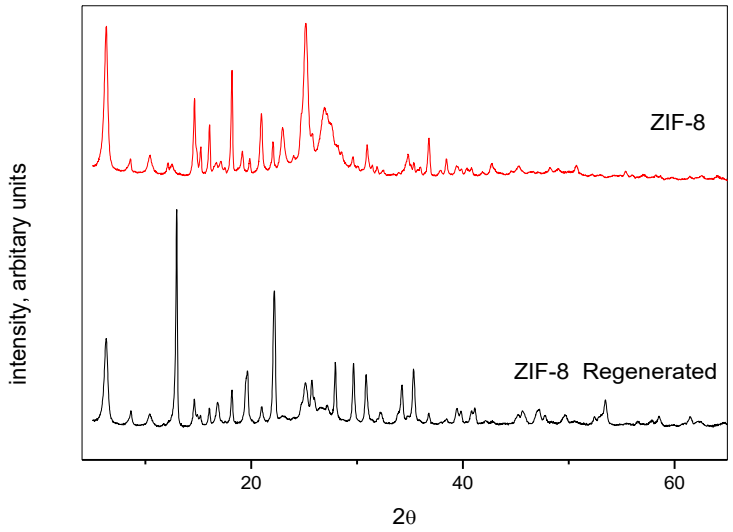

Fig. 24. X-ray diffraction spectra of ZIF-8 and regenerated ZIF-8.

4. Conclusions

In summary, the Zeolitic imidazolate framework-8 (ZIF-8) was successfully synthesized and proved to be an adsorbent with high efficiency. The morphology of the ZIF-8 is very uniform in spherical form, with an average particle size of 165 to 348 nm in diameter range. The ZIF-8 material has a very large surface area of BET 495.199 m^2/g and a total pore volume of 0.026 cm^3/g. Results indicated that CV and MG adsorption depended heavily on initial dye concentration, initial solution pH, contact time and temperature. The adsorption equilibrium showed that the Langmuir isotherm suited the experimental data better than the other models for both CV and MG dyes. The mean adsorption energy values (E_a) for CV and MG are 16.14 and 19.79 $kJmol^{-1}$, respectively suggesting a chemisorption process. The pseudo-second - order kinetic model, based on the correlation coefficient (R^2), was found to follow the adsorption kinetics. The thermodynamic parameters determined (ΔH^o, ΔS^o and ΔG^o) It showed that adsorption of both dyes onto ZIF-8 under

experimental conditions was spontaneous and endothermic. ZIF-8 has a strong reusability characteristic as it still represents more than 90 percent after the third run of the original capacity due to its highly effective. The ZIF-8, which features well-defined standard mesopores, high surface area, and crystalline frameworks, giving great potential for various types of applications is awaited.

References

[1] H. Jactel, F. Verheggen, D. Thiéry, A.J. Escobar-Gutiérrez, E. Gachet, N. Desneux, N.W. Group, Alternatives to neonicotinoids, J Environment international, 129 (2019) 423-429.

[2] B. Li, Y. Dong, M. Li, Z. Ding, Comparative study of different Fe (III)-carboxylic fiber complexes as novel heterogeneous Fenton catalysts for dye degradation, Journal of materials science, 49 (2014) 7639-7647.

[3] R. Mai, X. Wu, Y. Jiang, Y. Meng, B. Liu, X. Hu, J. Roncali, G. Zhou, J.-M. Liu, K. Kempa, An efficient multi-functional material based on polyether-substituted indolocarbazole for perovskite solar cells and solution-processed non-doped OLEDs, Journal of materials chemistry, 7 (2019) 1539-1547.

[4] S.A. Adebisi, O.S. Amuda, A.L. Adejumo, A.O. Olayiwola, A.G. Farombi, Equilibrium, kinetic and thermodynamics studies of adsorption of aniline blue from aqueous media using steam-activated carbon prepared from Delonix regia pod, Journal of Water Resource Protectio, 7(2015) 1221.

[5] S. Prateepchanachai, W. Thakhiew, S. Devahastin, S. Soponronnarit, Mechanical properties improvement of chitosan films via the use of plasticizer, charge modifying agent and film solution homogenization, J Carbohydrate polymers, 174 (2017) 253-261.

[6] K.S. Park, Z. Ni, A.P. Côté, J.Y. Choi, R. Huang, F.J. Uribe-Romo, H.K. Chae, M. O'Keeffe, O.M. Yaghi, Exceptional chemical and thermal stability of zeolitic imidazolate frameworks, J Proceedings of the National Academy of Sciences, 103 (2006) 10186-10191.

[7] S.K. Henninger, H.A. Habib, C. Janiak, MOFs as adsorbents for low temperature heating and cooling applications, Journal of the American Chemical Society, 131 (2009) 2776-2777.

[8] D. Wang, F. Jia, H. Wang, F. Chen, Y. Fang, W. Dong, G. Zeng, X. Li, Q. Yang, X. Yuan, Simultaneously efficient adsorption and photocatalytic degradation of tetracycline by Fe-based MOFs, Journal of colloid interface science, 519 (2018) 273-284.

[9] L. Li, L.J. Yuan, W. Hong, L. Fan, L.B. Mao, L. Liu, Hybrid Fe3O4/MOFs for the adsorption of methylene blue and methyl violet from aqueous solution, J Desalination Water Treatment, 55 (2015) 1973-1980.

[10] J. Yao, H. Wang, Zeolitic imidazolate framework composite membranes and thin films: synthesis and applications, J Chemical Society Reviews, 43 (2014) 4470-4493.

[11] Y. Feng, Y. Li, M. Xu, S. Liu, J. Yao, Fast adsorption of methyl blue on zeolitic imidazolate framework-8 and its adsorption mechanism, J RSC advances, 6 (2016) 109608-109612.

[12] N.M. Mahmoodi, S. Khorramfar, F. Najafi, Amine-functionalized silica nanoparticle: Preparation, characterization and anionic dye removal ability, J. Desalination, 279 (2011) 61-68.

[13] D. Kulkarni, I.E. Wachs, Isopropanol oxidation by pure metal oxide catalysts: number of active surface sites and turnover frequencies, J. Applied Catalysis A: General, 237 (2002) 121-137.

[14] F. Huang, Y. Xu, S. Liao, D. Yang, Y.-L. Hsieh, Q. Wei, Preparation of amidoxime polyacrylonitrile chelating nanofibers and their application for adsorption of metal ions, J. Materials, 6 (2013) 969-980.

[15] Y.S. Al-Degs, M.I. El-Barghouthi, A.H. El-Sheikh, G.M. Walker, Effect of solution pH, ionic strength, and temperature on adsorption behavior of reactive dyes on activated carbon, J. Dyes Pigments, 77 (2008) 16-23.

[16] M. He, J. Yao, Q. Liu, K. Wang, F. Chen, H. Wang, Facile synthesis of zeolitic imidazolate framework-8 from a

concentrated aqueous solution, J Chemical Society Reviews, 184 (2014) 55-60.
[17] Y. Hu, H. Kazemian, S. Rohani, Y. Huang, Y. Song, In situ high pressure study of ZIF-8 by FTIR spectroscopy, J Chemical Communications, 47 (2011) 12694-12696.
[18] D.E. Wurster, E. Oh, J.C. Wang, Determination of the mechanism for the decrease in zinc oxide surface area upon high-temperature drying, Journal of pharmaceutical sciences, 84 (1995) 1301-1307.
[19] Y.L. Chen, L.-C. Kuo, M.L. Tseng, H.M. Chen, C.-K. Chen, H.J. Huang, R.-S. Liu, D.P. Tsai, ZnO nanorod optical disk photocatalytic reactor for photodegradation of methyl orange, J Optics express, 21 (2013) 7240-7249.

[20] L.-S. Zhang, K.-H. Wong, H.-Y. Yip, C. Hu, J.C. Yu, C.-Y. Chan, P.-K. Wong, Effective photocatalytic disinfection of E. coli K-12 using AgBr− Ag− Bi2WO6 nanojunction system irradiated by visible light: the role of diffusing hydroxyl radicals, J Environmental science technology, 44 (2010) 1392-1398.
[21] A. El-Bindary, N. Hassan, M. El-Afify, Synthesis and structural characterization of some divalent metal complexes: DNA binding and antitumor activity, Journal of Molecular Liquids, 242 (2017) 213-228.
[22] S. Sadaf, H.N. Bhatti, M. Arif, M. Amin, F. Nazar, Adsorptive removal of direct dyes by PEI-treated peanut husk biomass: Box–Behnken experimental design, J Chemistry Ecology, 31 (2015) 252-264.
[23] M. Özacar, İ.A. Şengil, Adsorption of reactive dyes on calcined alunite from aqueous solutions, Journal of hazardous materials, 98 (2003) 211-224.
[24] C. Djilani, R. Zaghdoudi, F. Djazi, B. Bouchekima, A. Lallam, A. Modarressi, M. Rogalski, Adsorption of dyes on activated carbon prepared from apricot stones and commercial activated carbon, Journal of the Taiwan Institute of Chemical Engineers, 53 (2015) 112-121.
[25] M. Yu, Y. Han, J. Li, L. Wang, CO_2-activated porous carbon derived from cattail biomass for removal of malachite green dye and application as supercapacitors, J Chemical Engineering Journal, 317 (2017) 493-502.
[26] S. Wong, N.A.N. Yac'cob, N. Ngadi, O. Hassan, I.M. Inuwa, From pollutant to solution of wastewater pollution: Synthesis of activated carbon from textile sludge for dye adsorption, J Chinese Journal of Chemical Engineering, 26 (2018) 870-878.
[27] A.A. El-Bindary, M.A. Hussien, M.A. Diab, A.M. Eessa, Adsorption of Acid Yellow 99 by polyacrylonitrile/activated carbon composite: kinetics, thermodynamics and isotherm studies, Journal of Molecular Liquids, 197 (2014) 236-242.
[28] I. Langmuir, The constitution and fundamental properties of solids and liquids. II. Liquids, Journal of the American Chemical Society, 39 (1917) 1848-1906.
[29] I. Langmuir, The adsorption of gases on plane surfaces of glass, mica and platinum, Journal of the American Chemical Society, 40 (1918) 1361-1403.
[30] H. Freundlich, W. Heller, The adsorption of cis-and trans-azobenzene, Journal of the American Chemical society, 61 (1939) 2228-2230.
[31] M.M. Dubinin, E. Zaverina, L. Radushkevich, Sorption and structure of active carbons. I. Adsorption of organic vapors, J Zhurnal Fizicheskoi Khimii, 21 (1947) 151-162.
[32] M. Temkin, V. Pyzhev, Recent modifications to Langmuir isotherms, (1940).
[33] S.K. Lagergren, About the theory of so-called adsorption of soluble substances, J Sven. Vetenskapsakad. Handingarl, 24 (1898) 1-39.
[34] Y.-S. Ho, G. McKay, Sorption of dye from aqueous solution by peat, J Chemical engineering journal, 70 (1998) 115-124.
[35] J. Zeldowitsch, Über den mechanismus der katalytischen oxydation von CO an MnO2, J Acta physicochim. URSS,

1 (1934) 364-449.
[36] N. Hassan, A. Shahat, A. El-Daidamony, M. El-Desouky, A. El-Bindary, Synthesis and characterization of ZnO nanoparticles via zeolitic imidazolate framework-8 and its application for removal of dyes, Journal of Molecular Structure, (2020) 128029.
[37] M.H. Dehghani, A. Dehghan, A. Najafpoor, Removing Reactive Red 120 and 196 using chitosan/zeolite composite from aqueous solutions: Kinetics, isotherms, and process optimization, Journal of Industrial Engineering Chemistry, 51 (2017) 185-195.
[38] Y. Zhang, G. Huang, C. An, X. Xin, X. Liu, M. Raman, Y. Yao, W. Wang, M. Doble, Transport of anionic azo dyes from aqueous solution to gemini surfactant-modified wheat bran: synchrotron infrared, molecular interaction and adsorption studies, J Science of the Total Environment, 595 (2017) 723-732.
[39] R. Juang, F. Wu, R. Tseng, The ability of activated clay for the adsorption of dyes from aqueous solutions, J Environmental Technology, 18 (1997) 525-531.
[40] H. Nollet, M. Roels, P. Lutgen, P. Van der Meeren, W. Verstraete, Removal of PCBs from wastewater using fly ash, J Chemosphere, 53 (2003) 655-665.
[41] M. Fathi, A. Asfaram, A. Farhangi, Removal of Direct Red 23 from aqueous solution using corn stalks: isotherms, kinetics and thermodynamic studies, J Spectrochimica Acta Part A: Molecular Biomolecular Spectroscopy, 135 (2015) 364-372.
[42] C. Prasad, S. Karlapudi, P. Venkateswarlu, I. Bahadur, S. Kumar, Green arbitrated synthesis of Fe_3O_4 magnetic nanoparticles with nanorod structure from pomegranate leaves and Congo red dye degradation studies for water treatment, Journal of Molecular Liquids, 240 (2017) 322-328.
[43] N. Hassan, A. Shahat, A. El-Didamony, M. El-Desouky, A. El-Bindary, Mesoporous iron oxide nano spheres for capturing organic dyes from water sources, Journal of Molecular Structure, (2020) 128361.
[44] M. Doğan, Y. Özdemir, M. Alkan, Adsorption kinetics and mechanism of cationic methyl violet and methylene blue dyes onto sepiolite, J Dyes Pigments, 75 (2007) 701-713.
[45] C. Kannan, N. Buvaneswari, T. Palvannan, Removal of plant poisoning dyes by adsorption on Tomato Plant Root and green carbon from aqueous solution and its recovery, J Desalination, 249 (2009) 1132-1138.
[46] R. Kumar, R. Ahmad, Biosorption of hazardous crystal violet dye from aqueous solution onto treated ginger waste (TGW), J Desalination, 265 (2011) 112-118.
[47] F. Atmani, A. Bensmaili, N. Mezenner, Synthetic textile effluent removal by skin almonds waste, J. Environ. Sci. Technol, 2 (2009) 153-169.
[48] S. Senthilkumaar, P. Varadarajan, K. Porkodi, C. Subbhuraam, Adsorption of methylene blue onto jute fiber carbon: kinetics and equilibrium studies, Journal of colloid, 284 (2005) 78-82.
[49] S. Khattri, M. Singh, Colour removal from synthetic dye wastewater using a bioadsorbent, J Water, Air, Soil Pollution, 120 (2000) 283-294.
[50] M. Idrissi, Y. Miyah, Y. Benjelloun, M. Chaouch, Degradation of crystal violet by heterogeneous Fenton-like reaction using Fe/Clay catalyst with H_2O_2, Journal of Materials Environmental Science, 7(2016) 50-58.
[51] R. Ahmad, Studies on adsorption of crystal violet dye from aqueous solution onto coniferous pinus bark powder (CPBP), Journal of hazardous materials, 171 (2009) 767-773.
[52] S. Jain, R.V. Jayaram, Removal of basic dyes from aqueous solution by low-cost adsorbent: Wood apple shell (Feronia acidissima), J Desalination, 250 (2010) 921-927.
[53] Y.-S. Ho, W.-T. Chiu, C.-C. Wang, Regression analysis for the sorption isotherms of basic dyes on sugarcane dust, J Bioresource technology, 96 (2005) 1285-1291.

[54] A.B. Karim, B. Mounir, M. Hachkar, M. Bakasse, A. Yaacoubi, Adsorption/desorption behavior of cationic dyes on Moroccan clay: equilibrium and mechanism, Journal of Materials Environmental Science, 8(2017) 1082-1096.
[55] S. Chakraborty, S. Chowdhury, P.D. Saha, Adsorption of crystal violet from aqueous solution onto NaOH-modified rice husk, J Carbohydrate Polymers, 86 (2011) 1533-1541.
[56] B. Sarada, M.K. Prasad, K.K. Kumar, C.V.R. Murthy, Cadmium removal by macro algae Caulerpa fastigiata: Characterization, kinetic, isotherm and thermodynamic studies, Journal of Environmental Chemical Engineering, 2 (2014) 1533-1542.
[57] G.O. El-Sayed, Removal of methylene blue and crystal violet from aqueous solutions by palm kernel fiber, J Desalination, 272 (2011) 225-232.
[58] S. Lairini, K. El Mahtal, Y. Miyah, K. Tanji, S. Guissi, S. Boumchita, F. Zerrouq, The adsorption of Crystal violet from aqueous solution by using potato peels (Solanum tuberosum): equilibrium and kinetic studies, J. Mater. Environ. Sci, 8 (2017) 3252-3261.
[59] S. Banerjee, Y.C. Sharma, Equilibrium and kinetic studies for removal of malachite green from aqueous solution by a low cost activated carbon, Journal of Industrial Engineering Chemistry, 19 (2013) 1099-1105.
[60] I.D. Mall, V.C. Srivastava, N.K. Agarwal, I.M. Mishra, Adsorptive removal of malachite green dye from aqueous solution by bagasse fly ash and activated carbon-kinetic study and equilibrium isotherm analyses, J Colloids Surfaces A: Physicochemical Engineering Aspects, 264 (2005) 17-28.
[61] P. Janoš, Sorption of basic dyes onto iron humate, J Environmental science technology, 37 (2003) 5792-5798.
[62] M.S. Derakhshan, O. Moradi, The study of thermodynamics and kinetics methyl orange and malachite green by SWCNTs, SWCNT-COOH and SWCNT-NH_2 as adsorbents from aqueous solution, Journal of Industrial Engineering Chemistry, 20 (2014) 3186-3194.
[63] M. Rajabi, K. Mahanpoor, O. Moradi, Removal of dye molecules from aqueous solution by carbon nanotubes and carbon nanotube functional groups: critical review, J Rsc Advances, 7 (2017) 47083-47090.
[64] S. Tahir, N.J.C. Rauf, Removal of a cationic dye from aqueous solutions by adsorption onto bentonite clay, J Chemosphere, 63 (2006) 1842-1848.
[65] M.J. Iqbal, M.N. Ashiq, Adsorption of dyes from aqueous solutions on activated charcoal, Journal of Hazardous Materials, 139 (2007) 57-66.
[66] J. Liu, H. Yu, Q. Liang, Y. Liu, J. Shen, Q. Bai, Preparation of polyhedral oligomeric silsesquioxane based cross-linked inorganic-organic nanohybrid as adsorbent for selective removal of acidic dyes from aqueous solution, Journal of colloid interface science, 497 (2017) 402-412.